Available online at www.sciencedirect.com
SCIENCE DIRECT®
Nuclear Instruments and Methods in Physics Research B 242 (2006) 448–451
NIM B Beam Interactions with Materials & Atoms
www.elsevier.com/locate/nimb

Ion-beam implantation and cross-sectional TEM characterization of $Gd_2Ti_2O_7$ pyrochlore

Jie Lian [a], L.M. Wang [a], R.C. Ewing [a,*], L.A. Boatner [b]

[a] Departments of Geological Sciences and Materials Science and Engineering, University of Michigan, Ann Arbor, MI 48109-2104, USA
[b] Oak Ridge National Laboratory, Oak Ridge, TN 37831-6056, USA

Available online 19 September 2005

Abstract

Radiation effects in a wide range of pyrochlore compositions have been extensively investigated due to the potential application of pyrochlores as host matrices for the immobilization of actinides – particularly Pu. In this study, we have performed 1.0 MeV Kr^{2+} ion implantations in bulk samples of single crystal $Gd_2Ti_2O_7$ at room temperature at different ion fluences of 1.875, 3.125 and 5×10^{14} ions/cm^2. The microstructural evolution upon ion-beam implantation was examined by cross-sectional transmission electron microscopy (TEM). The critical amorphization dose at room temperature for 1 MeV Kr^{2+} implanted $Gd_2Ti_2O_7$ was determined to be ~0.143 dpa, which is significantly lower than the dose obtained by ion-irradiation under in situ TEM observation.
© 2005 Elsevier B.V. All rights reserved.

PACS: 61.82.−d; 61.80.Jh; 81.40.Wx; 72.80.Ng

Keywords: Pyrochlore; Ion implantation; Critical amorphization dose; Cross-sectional TEM

1. Introduction

Recently, there has been great interest in using materials with fluorite and fluorite-related structures, such as isometric pyrochlores, as potential host phases for the immobilization of actinides, particularly Pu [1–11]. Numerous ion-beam-irradiation studies [12–19] have been carried out to simulate the radiation damage resulting from the α-decay events of incorporated radionuclides. Both heavy- and light-ion irradiations were performed at controlled temperatures, and in situ irradiations, combined with TEM observation, were used to examine the microstructural evolution upon ion-beam damage. The critical amorphization dose, D_c, the irradiation dose required to fully amorphize a given pyrochlore composition, was determined as a function of temperature. In the present study, we have performed bulk sample implantations in $Gd_2Ti_2O_7$ single crystals at room temperature, and the resulting microstructural evolution was characterized by cross-sectional TEM. The baseline critical amorphization doses at room temperature are compared to those obtained by in situ TEM observations.

2. Experimental

A 1.0 MeV Kr^{2+} ion implantation in $Gd_2Ti_2O_7$ single crystals was performed at room temperature using tandem ion accelerator at Argonne National Laboratory at different fluences of 1.875, 3.125 and 5×10^{14} ions/cm^2. The radiation damage and microstructure change upon ion implantation were examined using cross-sectional and high-resolution TEM techniques with a JEOL JEM 2010F microscope. The damage profiles observed by cross-sectional TEM were compared with those simulated by SRIM-2000 code. A threshold displacement energy of 50 eV was employed for all of the atoms in the pyrochlore structure in the SRIM calculations. The critical amorphization dose in the unit of displacements per atom (dpa) was determined as the dose at the interface between the amorphous layer and crystalline matrix.

* Corresponding author. Tel.: +1 734 763 9295; fax: +1 734 647 5706.
E-mail address: rodewing@umich.edu (R.C. Ewing).

0168-583X/$ - see front matter © 2005 Elsevier B.V. All rights reserved.
doi:10.1016/j.nimb.2005.08.060

3. Results and discussion

Fig. 1 shows the cross-sectional TEM image of $Gd_2Ti_2O_7$ implanted by 1 MeV Kr^{2+} at a fluence of 1.875×10^{14} ions/cm^2. A complete amorphous layer with ~350 nm thick was created starting from the surface of the sample as a result of radiation damage, and no diffraction contrast was observed within this layer. (Note, the surface of $Gd_2Ti_2O_7$ is not shown in Fig. 1.) The formation of the amorphous layer was further evidenced by the complete loss of diffraction maxima in the corresponding SAED pattern. Below the amorphous layer, where the radiation damage may be less than the critical amorphization dose required to fully amorphize $Gd_2Ti_2O_7$, a highly damaged layer was created as indicated by mottled zones of dark contrast in the TEM image. Fig. 2 shows high-resolution TEM images acquired from different areas across the interface between the amorphous layer and crystalline substrate. The formation of a completely amorphous layer was further evidenced by the complete loss of lattice fringes when the damage level was above the critical amorphization dose, D_c. A concurrent process of ion-beam-induced pyrochlore-to-fluorite structural transition was observed in conjunction with the radiation-induced amorphization process. The pyrochlore-to-fluorite structural transition in ion implanted/irradiated pyrochlore compounds was induced by the disordering of cations occupying the A- and B-sites, as well as anion vacancies [4,12,13,16,20]. The pyrochlore and fluorite structures can be distinguished by the presence or absence of superlattice diffraction maxima (or weak diffraction spots) in SAED patterns. Additionally, nano-sized fluorite domains were embedded in the amorphous matrix, and the corresponding selected-area electron diffraction patterns show only the diffraction maxima of the fluorite structure with diffuse haloes (inset in the

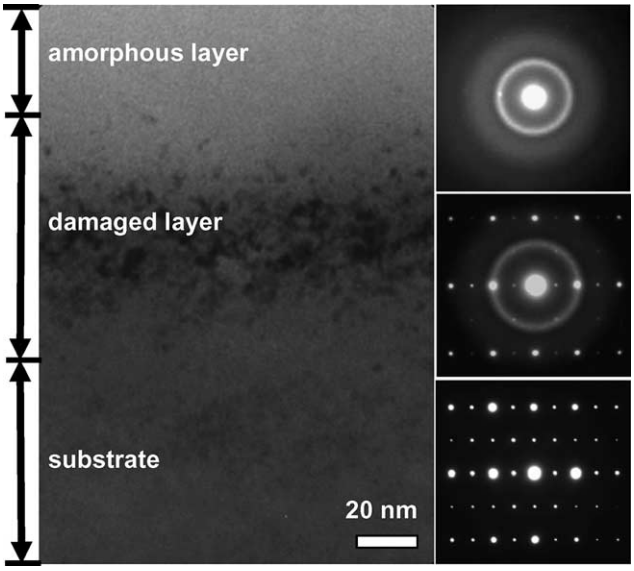

Fig. 1. Cross-sectional TEM image of a $Gd_2Ti_2O_7$ single crystal implanted by 1 MeV Kr^{2+} at room temperature at a fluence of 1.875×10^{14} ions/cm^2. The corresponding selected area electron diffraction patterns (SAED) were acquired from different areas across the damage layer.

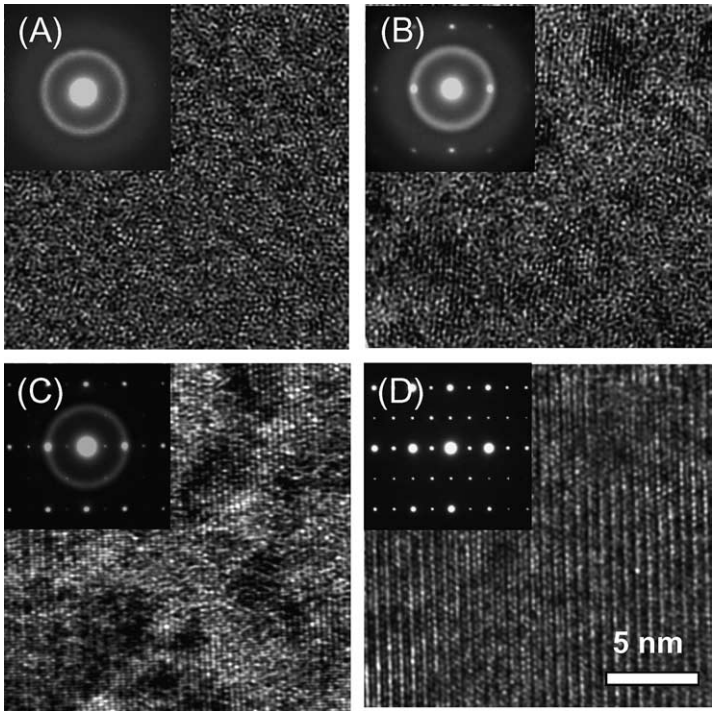

Fig. 2. High-resolution TEM (HRTEM) images across the damage profile of a $Gd_2Ti_2O_7$ single crystal implanted by 1 MeV Kr^{2+} at room temperature at a fluence of 1.875×10^{14} ions/cm^2. Different features, including a completely amorphous layer (A), fluorite domains in an amorphous matrix (B), amorphous domains embedded in the disordered-fluorite structure (C) and the ordered pyrochlore substrate (D), were observed.

Fig. 2(B)). Amorphous regions embedded in the crystalline matrix were also observed (Fig. 2(C)), suggesting that the amorphization process in ion-implanted $Gd_2Ti_2O_7$ occurs through a heterogeneous displacement process, instead of a homogeneous process in which a gradual increase of the point-defect concentration leads to a sudden change from a perfectly crystalline to an aperiodic material at a critical defect concentration.

An increase in the ion fluence thickens the amorphous layer (Fig. 3). The thicknesses of the amorphous layers of $Gd_2Ti_2O_7$ created by 1 MeV Kr^{2+} implantation at ion fluences of 3.125×10^{14} and 5×10^{14} ions/cm^2 are ~390 and ~410 nm, respectively. Full-cascade calculations using SRIM-2000 were performed with threshold displacement energies of 50 eV for all of the atoms in pyrochlore structure. The density (6.567 g/cm^3) of crystalline $Gd_2Ti_2O_7$ was used for SRIM calculations. Fig. 4 shows the simulated damage profiles at different ion fluences. By comparing the experimental damage profile with the simulated profile, the critical amorphization dose for 1 MeV Kr^{2+} implanted $Gd_2Ti_2O_7$ single crystals at ion fluences of 1.875, 3.125 and 5×10^{14} ions/cm^2 can be determined as ~0.14, ~0.142 and ~0.146 dpa, respectively. A consistent result for the critical amorphization dose for $Gd_2Ti_2O_7$ implanted by various ion fluences was obtained, indicating that ion implantation combined with cross-sectional TEM examination is particularly useful in investigating the microstructural evolution of materials upon ion-beam damage and determining the critical amorphization doses. A higher critical dose for $Gd_2Ti_2O_7$ at room temperature (~0.294 dpa) was obtained by in situ ion irradiation. During in situ TEM studies, a pre-thinned TEM foil was used for ion-beam irradiation. The high-surface-area to irradiated volume ratio and electron-beam radiation-enhanced annealing effects may lead to the migration and annihilation of isolated defects at the surface, resulting in an over estimation of the critical amorphization dose.

Using ~0.143 dpa as the average critical amorphization dose for 1 MeV Kr^{2+} implanted $Gd_2Ti_2O_7$ at room temperature, the amorphous layer simulated by SRIM-2000 code increases at higher ion fluences – as revealed by the dashed line in Fig. 4. This behavior is consistent with that determined by cross-sectional TEM observations. This result suggests that the increase in the amorphous layer thickness for 1 MeV Kr^{2+} implanted $Gd_2Ti_2O_7$ pyrochlore is due to the greater damage level accumulated at all depths across the cross-sectional damage profile at higher ion fluences (Fig. 4). We originally reported that ion implantation at high fluences thickens the amorphous layer in 300 keV Pb^+ implanted zircon crystals [21]. For the case of $ZrSiO_4$ crystals, there is a significant density decrease (up to 18%) with increasing α-decay dose and ion-beam radiation damage due to the swelling of amorphous zircon [22]. The growth of the amorphous layer in Pb^+ implanted zircon is mainly associated with the dimensional change caused by the volume expansion of amorphous zircon [21].

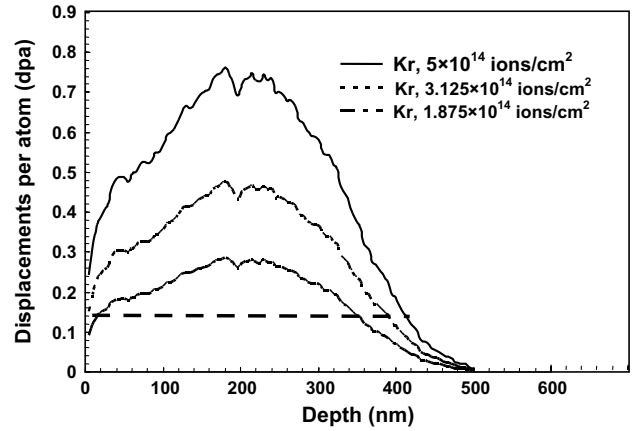

Fig. 4. Full-cascade calculated damage profiles for $Gd_2Ti_2O_7$ single crystals implanted by 1 MeV Kr^{2+} at room temperature at different ion fluences. The critical amorphization dose can be determined by comparing the experimental microstructure with the calculated damage profiles. The average critical amorphization dose of the $Gd_2Ti_2O_7$ single crystal subjected to 1 MeV Kr^{2+} implantation at room temperature is ~0.143 dpa, as shown by the dashed line in this figure.

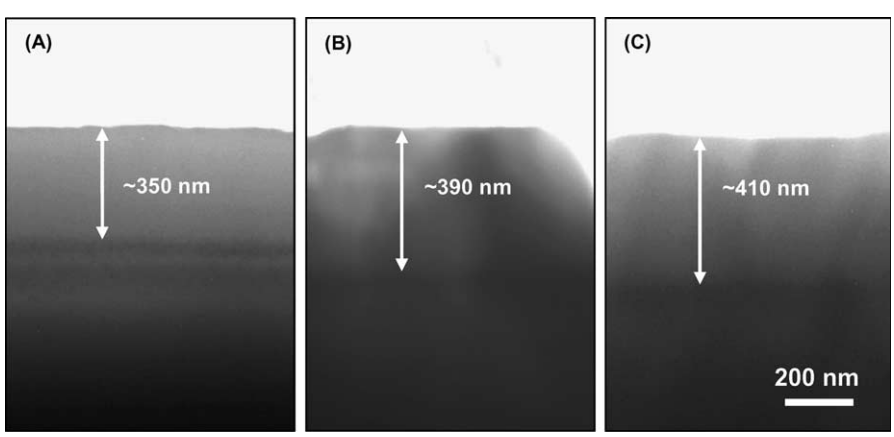

Fig. 3. Bright-field cross-sectional TEM images showing the damage profiles of $Gd_2Ti_2O_7$ single crystals implanted by 1 MeV Kr^{2+} at room temperature at different ion fluences: (A) 1.875, (B) 3.125 and (C) 5×10^{14} ions/cm^2. The thicknesses of the amorphous layers created by ion-beam damage are ~350, 390 and 410 nm, respectively.

Lumpkin et al. [23] studied the retention behavior of actinides in natural pyrochlores and zirconolites, and they reported systematic structural changes at doses between 2×10^{14} and 3×10^{17} α/mg. An important physical consequence of the displacive radiation damage is volume expansion which leads to microfracturing in coarse-grained (>100 μm) samples. In the present study, no significant volume expansion as a result of the radiation-induced amorphization was observed in the $Gd_2Ti_2O_7$ single crystal as evidenced by the well-defined thickness of the amorphous layer at different ion fluences, consistent with the results of the SRIM code simulations.

4. Conclusions

$Gd_2Ti_2O_7$ single crystals were implanted by 1 MeV Kr^{2+} ions at room temperature, and the microstructural evolution upon ion-beam damage was examined by cross-sectional TEM. The critical amorphization doses at room temperature were derived by comparing the experimental damage profiles with those simulated by the SRIM-2000 code. As a function of the radiation dose, different features were observed in the ion implanted titanate pyrochlore compounds including: a fully amorphous layer, domains of fluorite structure in an amorphous matrix, and amorphous regions embedded in the disordered fluorite structure and the ordered pyrochlore substrate. As the Kr^{2+} fluence increases from 1.875×10^{14} to 5×10^{14} ions/cm^2, the thickness of the amorphous layer created by ion-beam implantation increases slightly, and no significant volume expansion was observed as a result of ion-beam-induced amorphization. The critical amorphization dose at room temperature for 1 MeV Kr^{2+} implanted $Gd_2Ti_2O_7$ was determined to be ~0.143 dpa, i.e. a value that is significantly lower than the ion-irradiation dose found under in situ TEM observation conditions.

Acknowledgments

The authors thank the staff of the IVEM-Tandem Facility at the Argonne National Laboratory for assistance during ion implantation experiments. This work was supported by the Office of Basic Energy Sciences, USDOE under DOE grant DE-FG02-97ER45656. Oak Ridge National Laboratory is managed by UT-Battelle, LLC, for the USDOE under contract number DE-AC05-00OR22725.

References

[1] R.C. Ewing, W.J. Weber, J. Lian, J. Appl. Phys. 95 (2004) 5949.
[2] K.E. Sickafus, L. Minervini, R.W. Grimes, J.A. Valdez, M. Ishimaru, F. Li, K.J. McClellan, T. Hartmann, Science 289 (2000) 748.
[3] W.J. Weber, R.C. Ewing, Science 289 (2000) 2051.
[4] J. Lian, L.M. Wang, S.X. Wang, J. Chen, L.A. Boatner, R.C. Ewing, Phys. Rev. Lett. 87 (2001) 145901.
[5] W.J. Weber, R.C. Ewing, Mater. Res. Soc. Symp. Proc. 713 (2002) 443.
[6] K.B. Helean, A. Navrotsky, E.R. Vance, M.L. Carter, B. Ebbinghaus, O. Krikorian, J. Lian, L.M. Wang, J.G. Catalano, J. Nucl. Mater. 303 (2002) 226.
[7] K.B. Helean, S.V. Ushakov, C.E. Brown, A. Navrotsky, J. Lian, R.C. Ewing, J. Solid State Chem. 177 (2004) 1858.
[8] A.A. Digeos, J.A. Valdez, K.E. Sickafus, S. Atio, R.W. Grimes, A.R. Boccaccini, J. Mater. Sci. 38 (2003) 1597.
[9] P.E. Raison, R.G. Haire, Prog. Nucl. Energ. 38 (2001) 251.
[10] S.S. Shoup, C.E. Bamberger, R.G. Haire, J. Am. Ceram. Soc. 79 (1996) 1489.
[11] B.D. Begg, N.J. Hess, D.E. McCready, S. Thevuthasan, W.J. Weber, J. Nucl. Mater. 289 (2001) 188.
[12] S.X. Wang, B.D. Begg, L.M. Wang, R.C. Ewing, W.J. Weber, K.V.G. Kutty, J. Mater. Res. 14 (1999) 4470.
[13] S.X. Wang, L.M. Wang, R.C. Ewing, G.S. Was, G.R. Lumpkin, Nucl. Instr. and Meth. B 148 (1999) 704.
[14] B.D. Begg, N.J. Hess, W.J. Weber, R. Devanathan, J.P. Icenhower, S. Thevuthasan, B.P. McGrail, J. Nucl. Mater. 288 (2001) 208.
[15] A. Meldrum, C.W. White, V. Keppens, L.A. Boatner, R.C. Ewing, Phys. Rev. B 63 (2001) 104109.
[16] J. Lian, X.T. Zu, K.V.G. Kutty, J. Chen, L.M. Wang, R.C. Ewing, Phys. Rev. B 66 (2002) 054108.
[17] J. Lian, J. Chen, L.M. Wang, R.C. Ewing, J.M. Farmer, L.A. Boatner, K.B. Helean, Phys. Rev. B 68 (2003) 134107.
[18] J. Lian, R.C. Ewing, L.M. Wang, K.B. Helean, J. Mater. Res. 19 (2004) 1575.
[19] J. Lian, L.M. Wang, R.G. Haire, K.B. Helean, R.C. Ewing, Nucl. Instr. and Meth. B 218 (2004) 236.
[20] J. Lian, L. Wang, J. Chen, K. Sun, R.C. Ewing, J.M. Farmer, L.A. Boatner, Acta Mater. 51 (2003) 1493.
[21] J. Lian, S. Rios, L.A. Boatner, L.M. Wang, R.C. Ewing, J. Appl. Phys. 94 (2003) 5695.
[22] T. Murakami, B.C. Chakoumakos, R.C. Ewing, G.R. Lumpkin, W.J. Weber, Am. Mineral. 76 (1991) 1510.
[23] G.R. Lumpkin, K.P. Hart, P.J. McGlinn, T.E. Payne, Radiochim. Acta 66/67 (1994) 469.